Rap1-interacting adapter molecule (RIAM) associates with the plasma membrane via a proximity detector

Rap1-interacting adapter molecule (RIAM) associates with the plasma membrane via a proximity detector

Joseph P. Wynne,[1] Jinhua Wu,[2] Wenjuan Su,[1] Adam Mor,[1] Nikolaos Patsoukis,[3] Vassiliki A. Boussiotis,[3] Stevan R. Hubbard,[2] and Mark R. Philips[1]

[1]Cancer Institute and [2]Skirball Institute of Biomolecular Medicine, NYU School of Medicine, New York, NY 10016
[3]Division of Hematology and Oncology, Department of Medicine, Harvard Medical School, Boston, MA 02115

Adaptive immunity depends on lymphocyte adhesion that is mediated by the integrin lymphocyte functional antigen 1 (LFA-1). The small guanosine triphosphatase Rap1 regulates LFA-1 adhesiveness through one of its effectors, Rap1-interacting adapter molecule (RIAM). We show that RIAM was recruited to the lymphocyte plasma membrane (PM) through its Ras association (RA) and pleckstrin homology (PH) domains, both of which were required for lymphocyte adhesion. The N terminus of RIAM inhibited membrane translocation. In vitro, the RA domain bound both Rap1 and H-Ras with equal but relatively low affinity, whereas in vivo only Rap1 was required for PM association. The PH domain bound phosphoinositol 4,5-bisphosphate ($PI(4,5)P_2$) and was responsible for the spatial distribution of RIAM only at the PM of activated T cells. We determined the crystal structure of the RA and PH domains and found that, despite an intervening linker of 50 aa, the two domains were integrated into a single structural unit, which was critical for proper localization to the PM. Thus, the RA-PH domains of RIAM function as a proximity detector for activated Rap1 and $PI(4,5)P_2$.

Introduction

The adhesion of lymphocytes to vascular endothelium, extracellular matrix, and antigen-presenting cells (APCs) is critical to adaptive immunity and must be tightly regulated. Control of lymphocyte adhesion is accomplished, in large part, through the regulation of the principle adhesion molecule on the lymphocyte surface, the β2 integrin designated lymphocyte functional antigen 1 (LFA-1; Dustin et al., 2004). LFA-1 binds to intercellular adhesion molecule 1 (ICAM-1) on the surface of endothelium and APCs. Like other integrins, LFA-1 is an α/β heterodimeric transmembrane receptor that exists in multiple affinity states. The most adhesive state is thought to result from a conformational change in the receptor that extends the ectodomains of the α and β chains and is controlled by the disposition of the cytosolic domains (Schürpf and Springer, 2011). Talin, an actin binding protein, has been shown to interact with the β chain via its FERM domain and thereby activate integrins (Calderwood et al., 1999). Recruitment of talin is thought to represent the final step in signaling events within the lymphocyte that impinge on the cytosolic domains of the integrin, resulting in reorientation and enhanced adhesion of the ectodomains. This process is referred to as inside-out signaling (Kim et al., 2003; Mor et al., 2007) because most receptors on the cell surface convey information in the opposite direction.

The identity and mechanisms of action of the molecular components of inside-out signaling through LFA-1 is an intensely studied area. Among the few signaling molecules that have been implicated in the regulation of this process is Rap1, a small GTPase closely related to Ras. Expression of constitutively active Rap1 in lymphocytes induces LFA-1–mediated adhesion (Reedquist et al., 2000), and silencing (Ebisuno et al., 2010; Lafuente et al., 2004) or knockout (Duchniewicz et al., 2006) of Rap1a diminishes adhesion. Because small GTPases invariably

J.P. Wynne and J. Wu contributed equally to this paper.

Correspondence to Mark R. Philips: mark.philips@nyumc.org; or Stevan R. Hubbard: stevan.hubbard@nyumc.org

Jinhua Wu's present address is Developmental Therapeutics Program, Fox Chase Cancer Center, Philadelphia, PA 19111.

Abbreviations used in this paper: APC, antigen-presenting cell; ICAM-1, intercellular adhesion molecule 1; LFA-1, lymphocyte functional antigen 1; PH, pleckstrin homology; PIP, phosphoinositide phosphate; PM, plasma membrane; RA, Ras association; RIAM, Rap1-interacting adapter molecule; TCR, T cell receptor.

The Rockefeller University Press $30.00
J. Cell Biol. Vol. 199 No. 2 317–330
www.jcb.org/cgi/doi/10.1083/jcb.201201157

signal through effector molecules that bind to the GTPase only when it is GTP bound, there has been considerable interest in proteins that bind to GTP-loaded Rap1 in hematopoietic cells. Two such effectors have been identified using yeast two-hybrid screens. The first, RapL, was shown to regulate the clustering of LFA-1 at the leading edge of lymphocytes and at the immunological synapse (Katagiri et al., 2003), and RapL deficiency impairs lymphocyte adhesion and homing to secondary lymphoid organs (Katagiri et al., 2004). The second effector is Rap1-interacting adapter molecule (RIAM; Lafuente et al., 2004).

Overexpression of RIAM enhances lymphocyte adhesion, and silencing of RIAM inhibits Rap1-mediated LFA-1 activation (Lafuente et al., 2004). Moreover, the N-terminal region of RIAM binds talin (Lee et al., 2009). RIAM is a multidomain protein that includes a talin binding region, two coiled-coiled regions, two proline-rich regions, and sequential Ras association (RA) and pleckstrin homology (PH) domains (Fig. 2 A; Lafuente et al., 2004). The tandem RA-PH domains place RIAM in a family of proteins that also includes MIG-10, lamellipodin, and Pico, the so-called MRL family (Mig-10/RIAM/lamellipodin; Lafuente et al., 2004; Holt and Daly, 2005), which are related by the tandem RA-PH domains to the adaptor proteins Grb7/10/14. Because RA domains bind activated Ras-family GTPases that are associated with membranes and PH domains bind phosphoinositide phosphates (PIPs), which are constituents of the inner leaflet of the plasma membrane (PM), the RA-PH domains are considered to be a membrane-association module. Because RIAM must associate with the PM to regulate LFA-1, the function of the RA-PH domains should be critical to LFA-1 activation and therefore lymphocyte biology.

We have characterized the biochemical and structural features of the RA-PH domains that control the association of RIAM with the PM. Although the RA domain binds to both GTP-bound Rap1 and Ras in vitro with similar affinities, only Rap1 controls RIAM translocation in intact cells. The PH domain binds to $PI(4,5)P_2$. Both Rap1 and $PI(4,5)P_2$ binding are relatively low affinity, which explains why both are required for RIAM translocation. We determined the crystal structure of the RIAM RA-PH domains, which revealed that these two domains form a single structural entity that is critical for its function. Thus, the integrated RA-PH structure of RIAM acts as an AND gate to integrate Rap1 activation and $PI(4,5)P_2$ concentrations and as a proximity detector that restricts RIAM localization to the PM of activated cells.

Results

RIAM translocation to the PM in living cells

To study the ability of Rap1 to induce RIAM translocation to the PM in living cells, we tagged RIAM, or fragments thereof, with GFP and coexpressed these in Jurkat T cells with constitutively active mCherry-Rap1V12 (Fig. 1 A). As expected, mCherry-Rap1V12 was expressed both on the PM and internal membranes including the nuclear envelope. Neither full-length RIAM nor the RA domain expressed alone colocalized with mCherry-Rap1V12 but instead remained in the cytoplasm without decorating any membrane compartment. In contrast, the RA-PH domains expressed together with their endogenous linker but without the N and C terminus of RIAM (GFP-RA-PH) colocalized efficiently with mCherry-Rap1V12 at the PM (Fig. 1 A).

The inability to detect translocation of full-length, overexpressed GFP-RIAM to the PM by live cell imaging is concordant with results reported for other multidomain signaling proteins (Bondeva et al., 2002; Gureasko et al., 2008) and may relate to the relatively small fraction of the protein that interacts stably with the PM. To determine if endogenous RIAM translocates to the PM upon stimulation of Jurkat cells through the T cell receptor (TCR), we used nitrogen cavitation, subcellular fractionation, and immunoblot analysis (Fig. 1 B). Whereas all immunodetectable Rap1 was found in the membrane fraction, with or without stimulation, we found that the portion of endogenous RIAM detected in the membrane was small but increased from 1.7 ± 0.7 to $3.5 \pm 0.2\%$ ($n = 3$, $P < 0.02$) after stimulation. Thus, <2% of the total pool translocated. This result establishes that full-length RIAM does indeed translocate to membranes and also explains why it is difficult to detect translocation of overexpressed GFP-RIAM by imaging.

Strikingly, no colocalization of mCherry-Rap1V12 and GFP-RA-PH was observed on internal membranes. To determine if mCherry-Rap1V12 on internal membranes is accessible to probes that incorporate an efficient Rap1 binding domain, we also coexpressed mCherry-Rap1V12 with GFP-RalGDS-RBD (Ras binding domain) and observed efficient colocalization on all membranes decorated with mCherry-Rap1V12 (Fig. 1 A). These data indicate that expression of active Rap1 is sufficient to recruit GFP-RA-PH to the PM but not to internal membranes, and they suggest that translocation to the PM requires an additional determinant.

To determine if the RA-PH domains of RIAM are also restricted to the PM after physiological stimulation of lymphocytes through the TCR, we coexpressed in Jurkat T cells the GFP-RA-PH probe with wild-type Rap1 tagged with mCherry (Fig. 1 C). mCherry-Rap1 was distributed in a pattern indistinguishable from that of activated mCherry-Rap1V12 on both PM and internal membranes. In serum-starved Jurkat cells coexpressing mCherry-Rap1, GFP-RA-PH was expressed in the cytosol without decoration of any membrane. Within 2 min of stimulation with anti-CD3 antibodies, GFP-RA-PH translocated from the cytosol to the PM but not to endomembranes (Fig. 1 C). To verify that wild-type Rap1 becomes loaded with GTP on both the PM and internal membranes in response to stimulation, we used GFP-RalGDS-RBD as a probe for GTP-bound Rap1 and observed translocation to both the PM and internal membranes in response to cross-linking TCRs (Fig. 1 D). Thus, as was the case for expression of constitutively active Rap1, physiological stimulation of T cells through the TCR also led to activation of Rap1 on multiple membrane compartments but membrane recruitment of GFP-RA-PH was restricted to the PM.

To determine if the pattern of translocation of GFP-RA-PH is specific to lymphocytes, we performed an analogous experiment in COS-1 fibroblasts and found that, although mCherry-Rap1 was

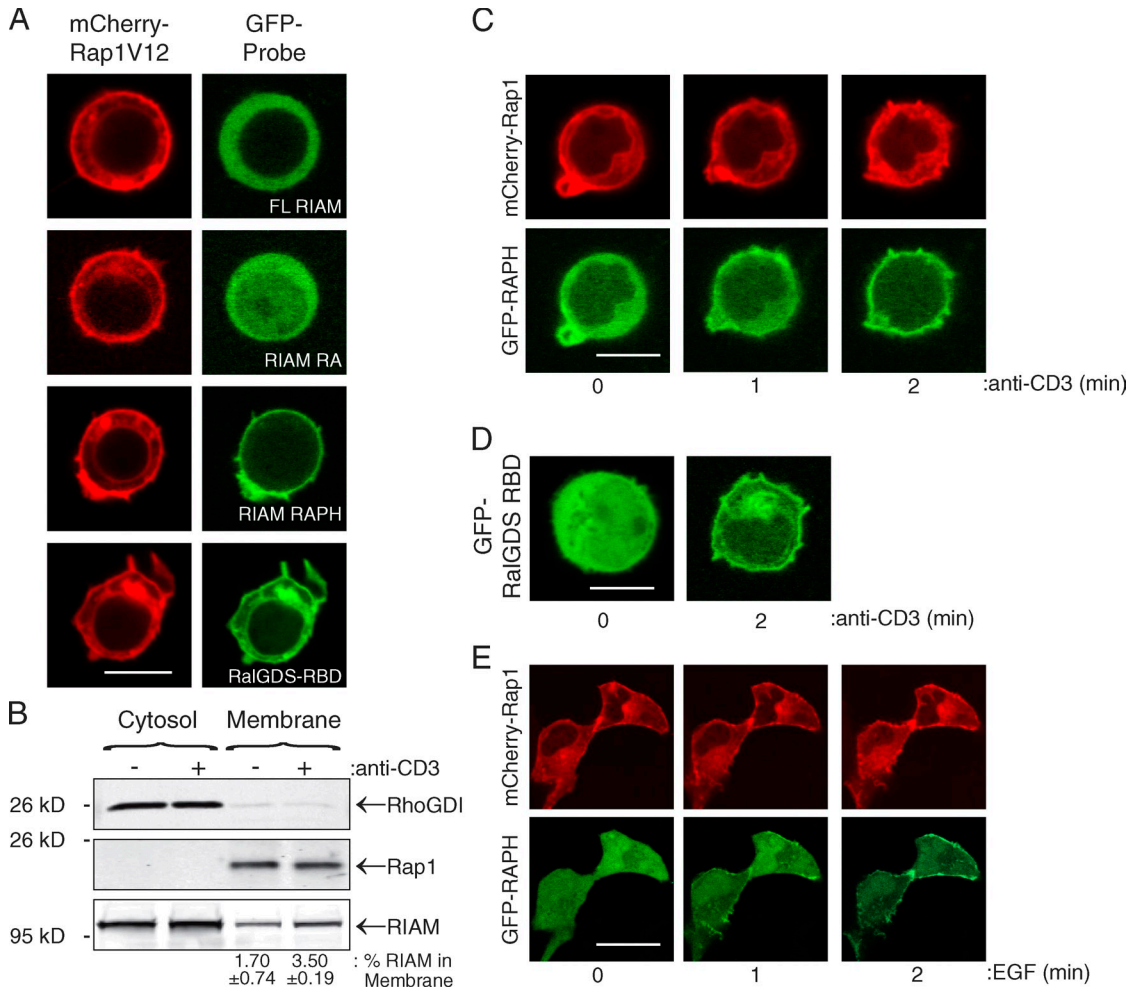

Figure 1. **RIAM translocation to the PM in live cells.** (A) GFP-tagged full-length (FL) RIAM, RIAM RA domain, RIAM RA-PH domains, or RalGDS-RBD (positive control probe for GTP-bound Rap1) were coexpressed in Jurkat T cells along with mCherry-tagged constitutively active Rap1V12 and the cells were imaged with a laser-scanning confocal microscope 24 h later. (B) Jurkat cells were homogenized by nitrogen cavitation before and after stimulation with anti-CD3 antibodies and membrane and cytosolic fractions were blotted for RIAM and RhoGDI (cytosolic control). Blots were quantified by Li-Cor and percent RIAM in the membrane fraction is indicated ($n = 3$, $P < 0.02$). (C and D) GFP-RA-PH (C) or GFP-RalGDS-RBD (D) was coexpressed with mCherry-tagged wild-type Rap1 in Jurkat T cells that were serum starved for 2 h and then imaged before and at the indicated times after the addition of cross-linking antibodies to CD3 (100 ng/ml). (E) The same experiment as in B substituting serum-starved COS-1 fibroblasts stimulated with 50 ng/ml EGF for the Jurkat T cells. Bars: (Jurkat cells) 5 µm; (COS-1 cells) 10 µm. Confocal images are representative of >80% of at least 20 cells imaged in at least three independent experiments.

expressed on both the PM and internal membrane of serum-starved cells, EGF stimulated GFP-RA-PH translocation only to the PM (Fig. 1 E). Together, these data show that although Rap1 is activated on multiple cellular membranes, the recruitment of its effector RIAM is restricted to the PM.

Autoinhibition by an N-terminal coiled-coil region

The markedly higher affinity of GFP-RA-PH relative to full-length GFP-RIAM for the PM of cells expressing GTP-bound Rap1 suggests that RA-PH is an efficient membrane targeting module that is inhibited by other regions of RIAM. To determine what portion of RIAM is responsible for inhibiting the translocation of full-length RIAM to the PM, we performed an analysis using a series of GFP-tagged deletion mutants (Fig. 2 A). Neither RIAM-GFP (Fig. 2 B) nor GFP-RIAM (Fig. 2 C) could be recruited to the PM by mCherry-Rap1V12 expression, indicating that the GFP tag was not responsible for the inhibition. Whereas RIAM lacking its C terminus (RIAM ΔCT) behaved like full-length RIAM and could not be recruited by mCherry-Rap1V12, RIAM lacking its N terminus (RIAM ΔNT) was recruited to the PM like GFP-RA-PH (Fig. 2 C). Thus, the RIAM N terminus inhibits the ability of the RA-PH domains to bind to the PM. Further analysis with additional truncation mutants (Fig. 2 C) mapped an inhibitory region to aa 29–57, which link the N-terminal talin binding region (aa 1–30) and the first of two N-terminal coiled-coil regions (aa 62–89). However, excision of aa 29–56 resulted in a construct that could not translocate to the PM, suggesting that, assuming proper folding of the domains flanking the deletion, the talin-binding domain is also inhibitory. These data suggest that the N-terminal region of RIAM, with or without the adjacent coiled-coil domain, might contribute to an intra- or intermolecular interaction that autoinhibits the molecule by blocking access to binding determinants at the PM.

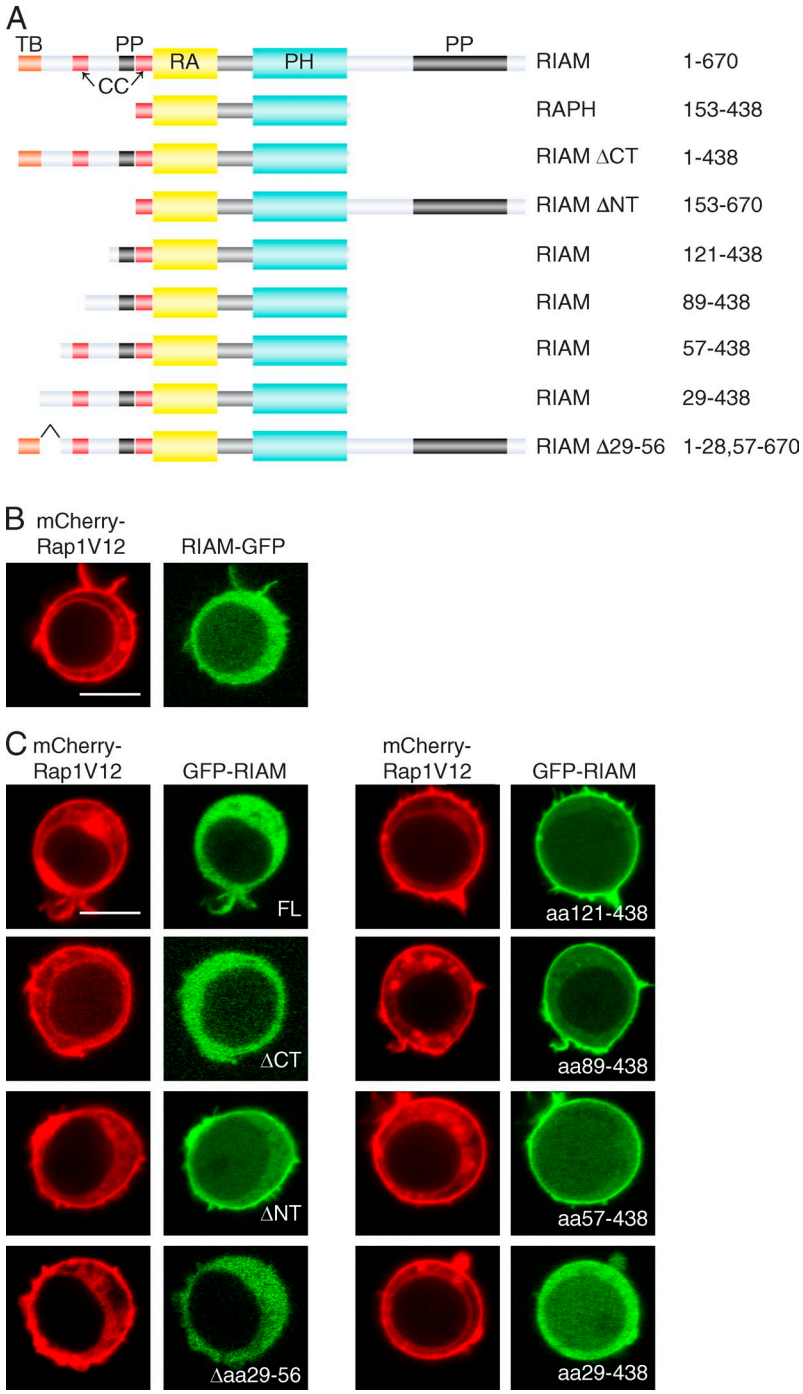

Figure 2. **The N terminus of RIAM inhibits translocation to the PM.** (A) The domain structure of RIAM includes a talin binding (TB) region, two coiled-coil (CC) regions, short and long polyproline (PP) regions, and the membrane targeting region consisting of RA and PH domains. The truncation mutants produced to analyze membrane association are aligned with full-length RIAM. (B) Co-expression of RIAM-GFP, tagged at the opposite end relative to GFP-RIAM, with constitutively active mCherry-Rap1V12 in Jurkat T cells. (C) Co-expression of GFP-RIAM or the indicated truncations with mCherry-Rap1V12 in Jurkat T cells. Bars: 5 µm.

Low affinity binding of the RA domain to activated Rap1

To study in vitro the interaction of RIAM with Rap1, we expressed GST-Rap1 in *Escherichia coli*, purified the fusion protein, loaded it with either GDPβS or GTPγS, and attempted affinity purification of GFP-RIAM or GFP-RA-PH from the lysate of COS-1 cells expressing the GFP-tagged proteins (Fig. 3, A and B). As a control, we expressed GFP-RalGDS-RBD, which is known to bind with high affinity to GTP-bound Rap1 (Bivona et al., 2004). GFP-RalGDS-RBD was affinity purified efficiently by 200 nM GST-Rap1 loaded with GTPγS. GTP-dependence was observed even at 4 µM GST-Rap1, demonstrating that the recombinant Rap1 was properly folded and capable of activation upon GTP binding (Fig. 3 A). GTP dependence was also observed with affinity capture of GFP-RA-PH. However, efficient pulldown of this protein was only achieved with 4 µM GST-Rap1 loaded with GTPγS (Fig. 3 A). Thus, although the RA domain of RIAM interacts in vitro with GTP-loaded Rap1, it does so with an affinity that is at least an order of magnitude less than that for binding to the RBD of RalGDS. GFP-RA-PH could also be affinity-purified to a similar extent by 4 µM GST-H-Ras loaded with GTPγS (Fig. 3 B). Full-length GFP-RIAM also bound to 4 µM GTP-loaded Rap1 and H-Ras, but to a much lesser degree than did GFP-RA-PH (Fig. 3 B). Importantly,

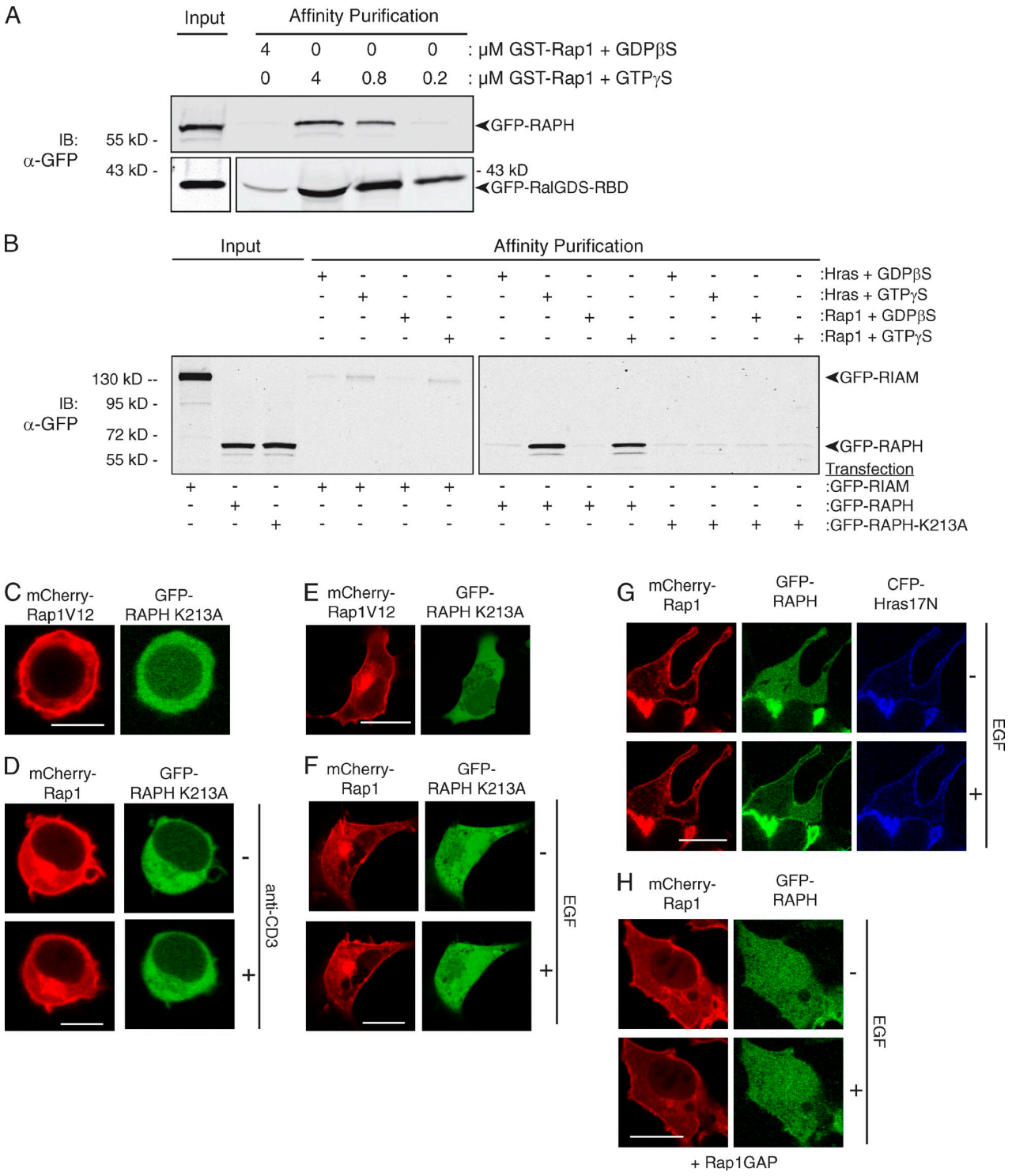

Figure 3. **RIAM RA domain binding to Rap1 is required for PM recruitment.** (A) Affinity purification of GFP-tagged RIAM RA-PH or RalGDS-RBD by the indicated concentrations of GST-tagged recombinant Rap1b loaded in vitro with either GDPβS or GTPγS. GFP fusion proteins were visualized by immunoblot for GFP. Immunoblots of the inputs are shown to the left. In the bottom panel, the input (lane 1) was run on a separate gel. The positions of the 55 or 43 kD markers are indicated for each gel. (B) Protein interaction assay as in A, tracking affinity purification of GFP-RIAM, GFP-RA-PH, and GFP-RA-PH K213A by 4 μM GDPβS- or GTPγS-loaded H-Ras or Rap1a. (A and B) the tiff images acquired with the Licor Odyssey were adjusted in Photoshop using the nonlinear Levels command. (C and E) Confocal localization of GFP-RA-PH with a K213A substitution predicted to inhibit RA function coexpressed with constitutively active mCherry-Rap1V12 in Jurkat T cells (C) or COS-1 cells (E). (D and F) Confocal localization of GFP-RA-PH coexpressed with wild-type mCherry-Rap1 in anti-CD3-stimulated Jurkat T cells (D) or EGF-stimulated COS-1 cells (F). (G) CFP-tagged dominant negative Hras17N, a potent and specific inhibitor of Ras signaling, was coexpressed in serum-starved COS-1 cells with GFP-RA-PH and mCherry-Rap1a and the cells were imaged before and after addition of EGF. (H) FLAG-Rap1GAP, a potent and specific inhibitor of Rap signaling, was coexpressed in serum-starved COS-1 cells with GFP-RA-PH and mCherry-Rap1 and the cells were imaged before and after addition of EGF. Bars: (Jurkat cells) 5 μm; (COS-1 cells) 10 μm.

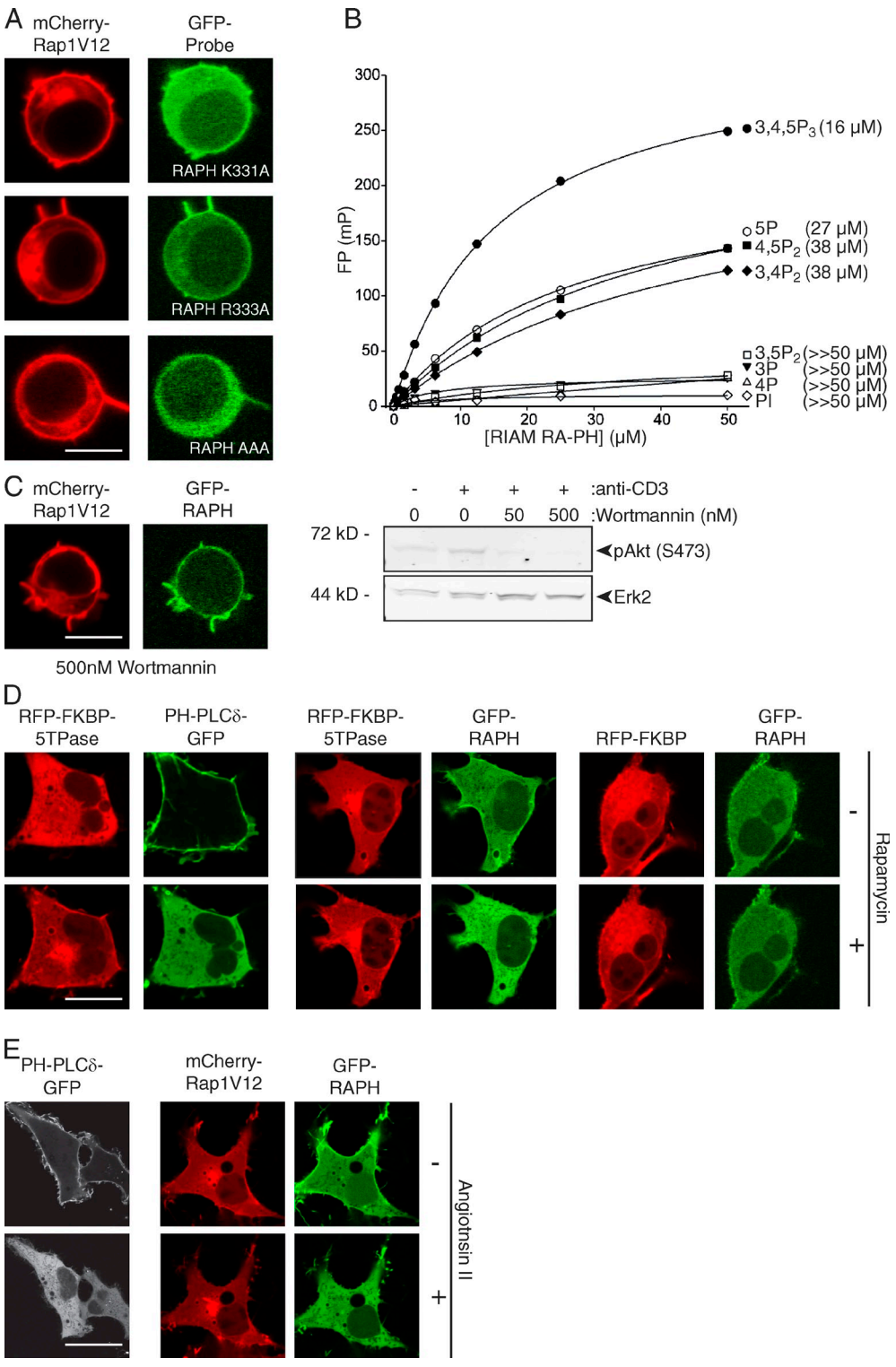

Figure 4. **RIAM PH domain binds PI(4,5)P_2.** (A) Colocalization in Jurkat T cells of mCherry-Rap1V12 and GFP-RA-PH with substitutions at the indicated basic amino acids that are predicted to be required for PIP binding. AAA indicates the triple mutation of K227A, K331A, and R333A. (B) Fluorescence polarization (FP) analysis of the binding of the indicated fluorescently labeled PIPs to recombinant RIAM RA-PH. K_d values obtained from the curve fittings are given on the right. As a result of the large protein demands of this experiment, it was performed once, although seven concentrations of RIAM RA-PH were measured independently for each PIP. (C) Effect of Wortmannin on Akt phosphorylation and GFP-RA-PH recruitment to PM in a Jurkat T cells coexpressing mCherry-Rap1V12. The tiffs shown in the immunoblot were adjusted in Photoshop with the nonlinear Levels command. The nearest molecular mass marker is shown to the left. (D) Localization of the PI(4,5)P_2 probe, PH-PLCδ-GFP, or GFP-RA-PH in COS-1 cells coexpressing Rap1V12, an FRB domain tethered to the PM, and a cytosolic PI(4,5)P_2-directed 5-phosphatase fused with FKBP12, before and after addition of rapamycin to induce heterodimerization of FKBP12 and FRB. (E) Localization of PH-PLCδ-GFP or GFP-RA-PH in COS-1 cells coexpressing mCherry-Rap1V12 and a Gq/PLCβ linked angiotensin II receptor before and after addition of angiotensin II. Bars: (Jurkat cells) 5 μm; (COS-1 cells) 10 μm.

when Lys213 in the Rap1 binding domain of GFP-RA-PH was mutated to alanine, a mutation predicted to disrupt the GTPase binding capacity of the RA domain (Kiel et al., 2005; Wohlgemuth et al., 2005), binding to both Rap1 and H-Ras was lost (Fig. 3 B). These data reveal that the RA domain binds GTP-bound Rap1, but at relatively low affinity, and that the binding activity is obtunded in full-length RIAM. The data also reveal that the RA domain of RIAM is potentially promiscuous with regard to Ras family GTPases because it binds equally well to Rap1 or H-Ras in vitro.

To confirm these biochemical findings in living cells, we studied the translocation of GFP-RA-PH in Jurkat T cells. The K213A substitution blocked translocation of GFP-RA-PH, both as a consequence of coexpression with mCherry-Rap1V12 (Fig. 3 C) and in response to TCR stimulation (Fig. 3 D). A similar effect was observed in COS-1 cells either expressing mCherry-Rap1V12 (Fig. 3 E) or wild-type mCherry-Rap1 and stimulated with EGF (Fig. 3 F).

Because in vitro H-Ras could substitute for Rap1 in RIAM RA-PH binding, we sought to determine which of these GTPases is relevant to RIAM translocation in living cells. The most effective way of shutting down Ras signaling without affecting Rap1 is to overexpress dominant-negative H-RasN17 (Stacey et al., 1991). Overexpression of H-RasN17 had no effect on the ability of mCherry-Rap1–expressing COS-1 cells to recruit GFP-RA-PH to the PM in response to EGF (Fig. 3 G), suggesting that Ras activation is not required for RIAM recruitment. In contrast, overexpression of Rap1GAP, a potent and specific negative regulator of Rap1, completely blocked translocation (Fig. 3 H). These data suggest that Rap1 but not Ras activation is required for RIAM translocation and strongly implicate Rap1 in the physiological regulation of this effector protein.

Low affinity binding of the PH domain to PI(4,5)P_2

Having implicated the RA domain and Rap1 in RIAM translocation to the PM, we next analyzed the contribution of the PH domain. The amino acid sequence in the β1-β2 loop region (see Crystal structure of the RIAM RA-PH domains) of the PH domain of RIAM conforms to the consensus K-X_n-(K/R)-X-R sequence (where X is any amino acid), which is associated with PIP binding (Isakoff et al., 1998). Mutation of K331 or R333 to alanine within this sequence resulted in diminished GFP-RA-PH recruitment to the PM in mCherry-Rap1V12–expressing cells, and mutation of both of these residues in combination with K327 completely abrogated translocation (Fig. 4 A).

Using various fluorescently labeled PIPs, recombinant RIAM RA-PH, and fluorescence polarization, we measured the binding of PIPs to the protein. No PIP bound with high affinity but several bound in the 16–38 µM range. Of these, PI(3,4,5)P_3 bound best (K_d = 16 µM), although PI5P, PI(4,5)P_2, and PI(3,4)P_2 bound nearly as well with K_d values = 27–38 µM (Fig. 4 B). Although Wortmannin inhibited Akt phosphorylation in TCR-stimulated Jurkat T cells, it had no effect on the translocation of GFP-RA-PH to the PM (Fig. 4 C), suggesting that PI3K activity is not necessary and that the marginally

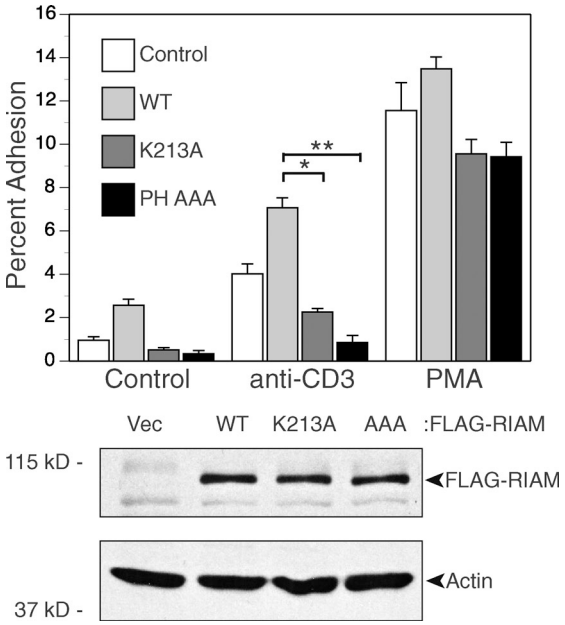

Figure 5. **Functional RA and PH domains are required for adhesion.** Jurkat T cells were electroporated with the indicated constructs and allowed to recover for 48 h. Cells were fluorescently labeled with BCECF, treated with or without 5 µg/ml anti-CD3 or 100 ng/ml PMA for 30 min at 37°C and allowed to adhere to ICAM-1–coated wells. After gentle washing of nonadherent cells, percent adhesion was determined by comparing input fluorescence to remaining fluorescence. Data shown are mean ± SEM, $n = 3$ (*, $P < 0.02$; **, $P < 0.0005$). The immunoblot in the lower panel shows equivalent expression of each RIAM construct. The nearest molecular mass marker is shown to the left.

stronger interaction of RA-PH with (the scarce) PI(3,4,5)P_3 has no physiological relevance. PI(4,5)P_2 is present in the PM at much higher concentrations than PI5P or PI(3,4)P_2 (Lemmon, 2008), making this PIP the most likely physiological target for the RIAM PH domain.

To investigate the relevance of PI(4,5)P_2, we used a fluorescent biosensor for this PIP, PH-PLCδ-GFP, an enzyme which degrades PI(4,5)P_2 and the FKBP12/rapamycin/FRB-induced protein dimerization methodology (Fig. 4 D). We expressed the catalytic domain of a PI(4,5)P_2-directed 5-phosphatase fused with both RFP and FKBP12 in cells that also expressed the FRB rapamycin binding domain of mTor at the PM (Varnai et al., 2006). In untreated cells, PH-PLCδ-GFP decorated the PM indicating that, as expected, this is a compartment enriched in PI(4,5)P_2. Addition of rapamycin induced rapid (<2 min) loss of PH-PLCδ-GFP from the PM, indicating that the induced dimerization system worked to rapidly dephosphorylate PI(4,5)P_2. Under the same conditions, GFP-RA-PH was lost from the PM, indicating that PI(4,5)P_2 is a physiologically relevant ligand for the RIAM PH domain. We confirmed this observation by engineering COS-1 cells to express angiotensin II receptors. This receptor engages G proteins that are coupled to PLCβ, which also catabolizes PI(4,5)P_2 (Várnai and Balla, 1998). Addition of angiotensin II to these cells induced a rapid loss of PH-PLCδ-GFP from the PM and blocked the recruitment of GFP-RA-PH to the PM (Fig. 4 E). Together, these data indicate that the PH domain of RIAM is functional, is required for binding to the PM, and binds PI(4,5)P_2 at this location.

Table 1. **X-ray data collection and refinement statistics**

Variable	Value
Data collection	
Space group	$P2_1$
Cell dimensions	
a, *b*, *c*	46.86, 82.39, and 83.40Å
α, β, γ	90, 95.2, and 90°
Wavelength	0.9790
Resolution	50.0–2.35Å
R_{sym} or R_{merge}	5.9 (27.5)[a]
$I/\sigma I$	19 (3.2)[a]
Completeness	91.7% (98.3%)[a]
Redundancy	2.9
Refinement	
Resolution	2.35Å
No. reflections	22,885
R_{work}/R_{free}	23.0/27.5
Number of atoms	
Protein	4,004
Solvent	260
B factors	
Protein	17.5
Solvent	21.2
R.m.s deviations	
Bond lengths	0.006Å
Bond angles	0.88°

[a]Values in parentheses are for the highest resolution shell (2.35–2.41 Å). One crystal was used for each data set. TLS (translation/libration/screw) parameters, one set for each protomer, were included in the refinement.

Functional RA and PH domains of RIAM are required for T cell adhesion

Having defined the binding parameters of both the RA and PH domains, we next sought to determine if both are required for stimulated lymphocyte adhesion. We transduced Jurkat T cells with either wild-type RIAM or RIAM with the mutations we defined as inhibiting the RA or PH domains. Overexpressed wild-type RIAM stimulated slightly basal adhesion of Jurkat T cells to ICAM-1–coated plates and significantly increased adhesion after stimulation of the TCR (Fig. 5). In contrast, neither the K213A RA domain mutant nor the K327,331,333A (AAA) PH domain mutant supported increased adhesion. Indeed, these mutants reduced adhesion below the level of the vector control, suggesting that they function as dominant-negative proteins. These data demonstrate that both a functional RA and PH domain are required for RIAM-supported adhesion.

Crystal structure of the RIAM RA-PH domains

To better understand the molecular basis for the interactions of RIAM with its binding partners, we determined the crystal structure of the RA-PH domains of mouse RIAM (residues 149–437). Crystals of this protein were obtained in monoclinic space group $P2_1$ with two RIAM RA-PH molecules in the asymmetric unit. The structure was determined by molecular replacement, using the Grb10 RA-PH structure (Depetris et al., 2009; PDB accession no. 3HK0) as a search model. Data collection and refinement statistics (at 2.35 Å) are given in Table 1.

Like the corresponding domains in Grb10, the RA and PH domains of RIAM adopt the canonical folds of their respective families yet form a single structural unit through an extensive RA-PH domain interface, which is further fortified by interactions from residues in the intervening linker region (Fig. 6 A). At its C terminus, the PH domain of RIAM contains a noncanonical C-terminal helix, α-helix 2 (α2), which packs against the RA domain. In Grb10, this helix mediates dimerization of RA-PH (Depetris et al., 2009) but is not observed to do so in the RIAM RA-PH structure. The two molecules of RIAM RA-PH in the asymmetric unit of the crystal are related by a molecular twofold axis, but the buried surface area in this dimer is modest (1,178 $Å^2$), indicating that this dimer is probably not relevant in vivo.

Based on the crystal structures of other GTPase–RA domain complexes (Nassar et al., 1995; Huang et al., 1998), residues in and flanking β2 (Fig. 6, A and B, red) will be the primary contacts

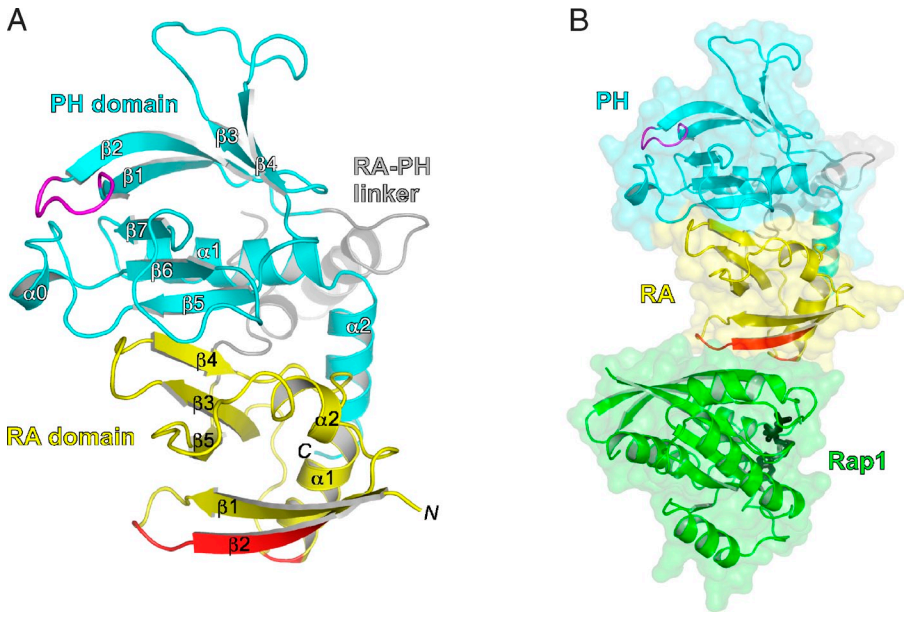

Figure 6. **Crystal structure of the RA-PH domains of mouse RIAM.** (A) Ribbon diagram of the crystal structure of RIAM RA-PH. The RA domain is colored yellow, the PH domain is colored cyan, and the intervening linker is colored gray. Residues in the RA domain that are predicted to interact with active GTPases are colored red, and the β1-β2 loop in the PH domain, the presumed site of PIP binding, is colored magenta. Secondary-structure elements (α helices and β strands) within the RA and PH domains are labeled, as are the N and C termini. (B) Model of the interaction between RIAM RA-PH and GTP-loaded Rap1. The model is based on the crystal structure of Grb14 RA-PH bound to H-Ras (not depicted). The same orientation and coloring as in A is shown, with Rap1 colored green and GTP colored black and shown in stick representation. The figure is rendered with PyMOL.

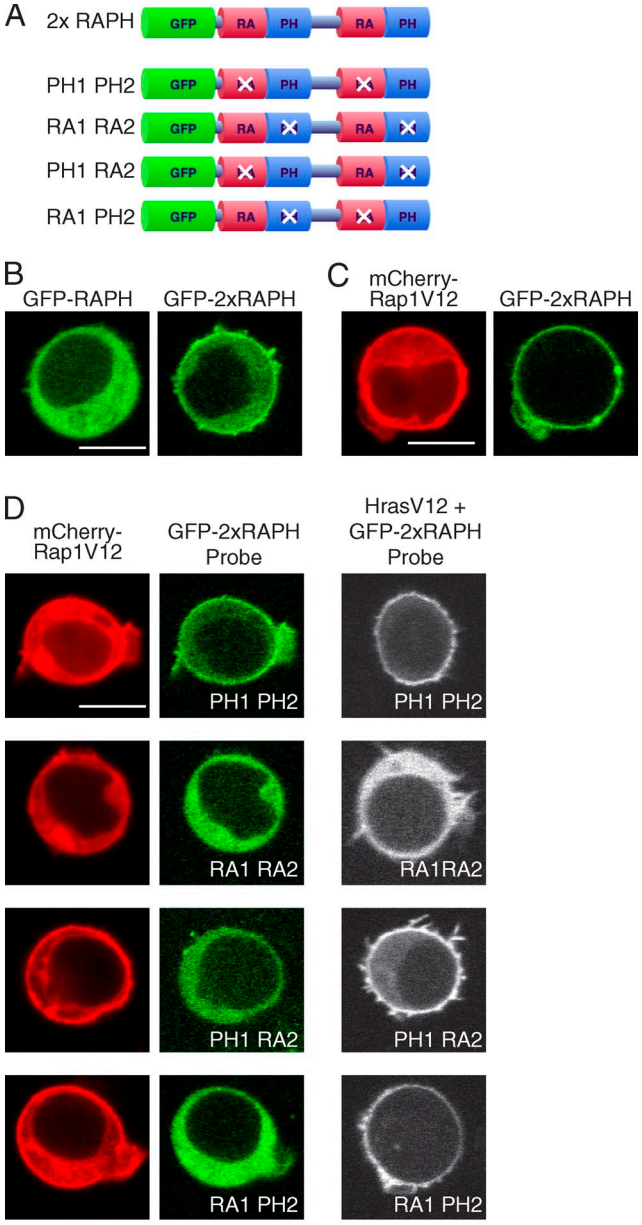

E

Plasma Membrane Recruitment of GFP-RAPH Probe			
Probe	Alone	With Active Rap1	With Active Hras
RAPH	–	+	+
2xRAPH	+	+	+
2xRAPH PH1 PH2	–	+	+
2xRAPH RA1 RA2	–	–	–
2xRAPH PH1 RA2	–	–	+
2xRAPH RA1 PH2	–	–	+

Figure 7. **Integrated structure of the RA-PH domains is required for PM association of RIAM.** (A) Schematic representation of RIAM RA-PH domain tandem probes used in B–E. An X through a domain indicates that it has been inactivated by mutation (K213A for RA and K327A/K331A/R333A for PH). (B and C) Localization of GFP-2xRAPH expressed alone in Jurkat T cells (B) or with mCherry-Rap1V12 (C). (D) Localization of the indicated GFP-tagged tandem RA-PH probes in Jurkat T cells coexpressing mCherry-Rap1V12 at near endogenous levels or active HrasV12 expressed 10–100-fold above endogenous (grayscale images to right). (E) Chart summarizing PM recruitment. Bars: 5 µm.

between the RIAM RA domain and the switch 1 region of active Rap1. Lys213 in α1 of the RIAM RA domain is predicted to interact with Asp33 of Rap1. Mutation of this lysine abrogated co-localization of GFP-RA-PH with Rap1 at the PM (Fig. 3, C–F).

In the RIAM PH domain, β2 and the preceding β1-β2 loop contain several lysine and arginine residues (K-X_n-(K/R)-X-R) that are likely to engage the negatively charged headgroup of PI(4,5)P_2. The presence of Arg333 in β2, mutation of which compromises RA-PH translocation to the PM (Fig. 4 A), suggests that the PIP headgroup will bind canonically "atop" the β1-β2 loop (Ceccarelli et al., 2007; Depetris et al., 2009).

Structural integration of RA and PH domains is required for their function

We sought to determine whether the integrated structure of the RIAM RA-PH domains was functionally significant. Because of the unlikelihood of obtaining independently folded and functional RA and PH domains by mutating the domain interface (not depicted), we instead took the approach of engineering a tandem RA-PH-domain protein and abolishing domain functionality individually via point mutation, effectively creating a "beads-on-a-string" configuration (Fig. 7 A).

GFP-2xRA-PH had higher affinity for the PM of Jurkat cells than did GFP-RA-PH because a significant portion of the tandem probe localized at the PM even in resting cells (Fig. 7 B). Co-expression with GTP-bound mCherry-Rap1V12 induced robust recruitment to the PM without any probe remaining in the cytosol (Fig. 7 C). Thus, the tandem probe is functional, and the higher valence leads to higher avidity for the PM. Interestingly, mutation of both RA domains in the tandem construct resulted in a probe that localized to the PM in cells expressing mCherry-Rap1V12, suggesting that tandem, dimeric PH domains afford sufficient affinity for PI(4,5)P_2 to affect binding, even in the absence of an interaction with a GTPase (Fig. 7, D and E). In contrast, mutation of both PH domains yielded a probe that could not be recruited to the PM (Fig. 7, D and E). Expression of active H-Ras12V from a pCGN vector resulted in expression levels >10-fold that of mCherry-Rap1V12 (unpublished data). Even at this level of expression, H-Ras12V was unable to recruit the dimeric RA domains without a functional PH domain. These data argue that the PH domain is the more important domain of the two for PM localization. When one RA and one PH domain were mutated so as to present one active copy of each domain separated from the other on the same polypeptide, mCherry-Rap1V12 failed to recruit the probe to any membrane (Fig. 7, D and E). Overexpressed H-Ras12V was capable of recruiting the probe, indicating that the binding domains were properly folded and functional. These data demonstrate that the structural unity of the RA and PH domains, as revealed by their crystal structure, is crucial for the ability of RIAM to interact with GTP-Rap1 and physiological levels of PI(4,5)P_2 at the PM.

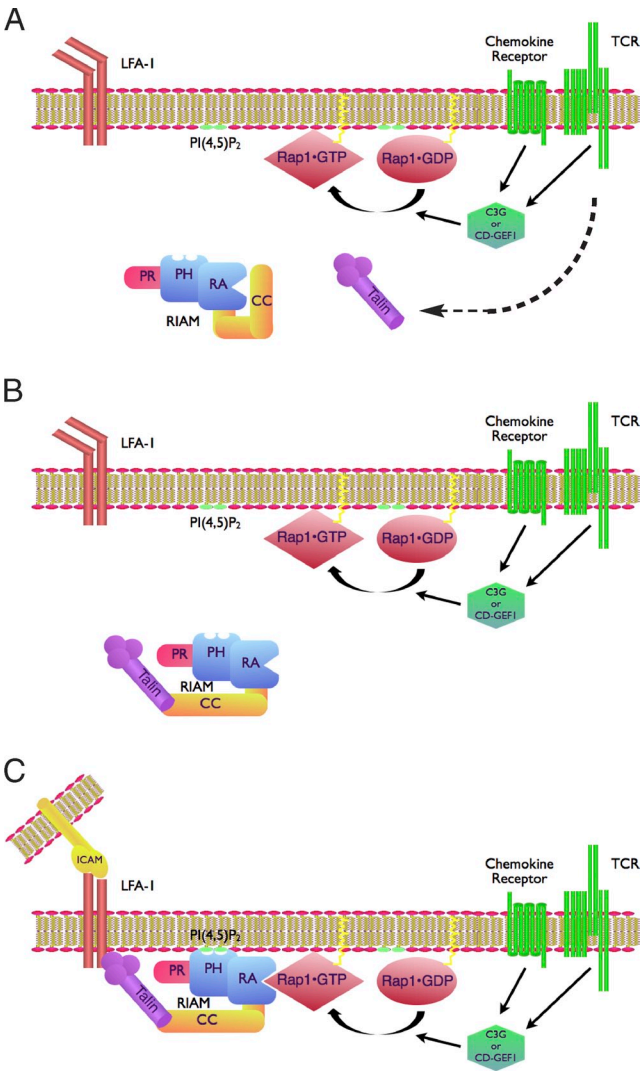

Figure 8. **Model for RIAM translocation to the PM of lymphocytes.** Although Rap1 constitutively associates with multiple cellular membranes by virtue of its geranylgeranyl modification, the relevant pool for LFA-1 regulation is at the PM where it is activated by one of two GEFs, C3G or CD-GEF1, that are downstream of both the TCR and chemokine receptors (A). In the resting state, RIAM is cytosolic and its N terminus inhibits the RA-RH membrane association domains. This inhibition may be alleviated by the interaction of talin with its binding region at the N terminus of RIAM (B). The exposed RA-PH domain is now free to associate with the PM where the RA-PH domains can sense the coincidence of GTP-bound Rap1 and the constitutively high concentrations of $PI(4,5)P_2$ (C). The domains are not drawn to scale. In particular, the C terminus that includes the proline rich (PR) region is reduced.

Discussion

Effectors of small GTPases are defined as signaling molecules that bind to the GTPase only when it is in the GTP-bound configuration and, in so doing, affect a change that conveys signaling information. The signaling information may be allosteric regulation of the effector, if it is an enzyme, or recruitment of the effector to the relevant subcellular compartment. In the case of RIAM, it appears that relocalization from the cytosol to the PM is the principle function of its RA domain. This is also true for the best studied Ras effector, Raf-1, which is recruited to the PM via its RA domain/RBD. In the case of Raf-1, it is clear that the RBD itself is necessary and sufficient to drive Raf-1 to membranes decorated with activated GTP-bound Ras (Chiu et al., 2002). In contrast, our data show that the RA domain of RIAM is not sufficient but requires an additional contribution from a PH domain that is structurally integrated with the RA domain.

Our inability to detect PM translocation of full-length GFP-tagged RIAM to the PM of Jurkat cells by live cell imaging cannot be interpreted as indicating that endogenous RIAM does not associate with the PM. This is a common result with GFP-tagged, overexpressed, multidomain signaling proteins because when the pool that translocates is small relative to the vast amount that remains in the cytosol, it is difficult to score for PM enhancement by fluorescence. This is the case for PM recruitment of the Ras effector Raf-1 (Bondeva et al., 2002; Chiu et al., 2002). Our analysis of endogenous RIAM by subcellular fractionation (Fig. 1 B) confirms that only a small portion of the protein stably associates with membranes in stimulated cells.

Both Ras and Rap proteins are present on multiple subcellular compartments (Choy et al., 1999; Bivona et al., 2004). The RA domains of Raf-1 and RalGDS bind Ras and Rap, respectively, with relatively high affinity and have been shown to colocalize with the activated form of the GTPase on all membrane compartments on which they are expressed (Chiu et al., 2002; Bivona et al., 2004). This observation has led to the recognition that Ras proteins signal from multiple subcellular compartments and that the signal output differs from each localization, providing an additional level of signaling complexity (Chiu et al., 2002). Our data show that, in contrast, signaling through RIAM is restricted to only one of the compartments upon which GTP-bound Rap1 accumulates. The affinity of the RIAM PH domain for $PI(4,5)P_2$, a PIP which is enriched only in the inner leaflet of the PM, explains the spatial restriction of RIAM membrane association. Whereas Raf-1 regulates MEK/Erk kinases, which have roles both at the PM and in the cytoplasm (Torii et al., 2004), RIAM regulates LFA-1, which functions only at the PM. Thus, the spatial restriction afforded by combining a relatively low affinity RA domain with a $PI(4,5)P_2$-directed PH domain would provide efficiency by bringing RIAM only to the subcellular localization where it is needed.

RA domains/RBDs possess a ubiquitin fold and typically bind to Ras proteins through an inter-protein β-sheet stabilized by electrostatic interactions (Emerson et al., 1995; Nassar et al., 1995). Importantly, the binding affinities for GTP-bound GTPases vary widely, with K_d values that range from 80 nM for Raf-1/Ras to 4 µM for RIN1/Rap1 (Wohlgemuth et al., 2005). Our in vitro pulldown experiments (Fig. 3, A and B) show that RIAM RA-PH binds to GTP-loaded Rap1 or H-Ras with relatively low and approximately equal affinities. Previous structural and mutagenesis studies pinpointed residue 31—Glu31 in Ras and Lys31 in Rap1—as a key specificity determinant in the binding of the RA domains of Raf-1 and RalGDS (Nassar et al., 1996). Lys84 (α1) in the Raf-1 RA domain interacts electrostatically with Glu31 of Ras, and Asp56 (α1-β3 loop) in RalGDS interacts electrostatically with Lys31 of Rap1. In RIAM and the other RA-PH proteins, the residues corresponding to Lys84 (Raf-1) and Asp 56 (RalGDS) are not charged (and not conserved), providing a rationale as to why the RA-PH proteins are less discriminating in binding to Ras versus Rap1.

The crystal structure of the RIAM RA and PH domains shows that these two domains, separated in sequence by ∼50 residues, nevertheless physically associate through a conserved interface to form a single structural unit. This feature was also observed in the crystal structure of the RA-PH domains of Grb10 (Depetris et al., 2009), suggesting that it will be a general feature of the MRL and Grb7/10/14 protein families.

The integrated structural nature of the RA-PH domains (and the hydrophobic interface) suggests that they are unlikely to fold properly when expressed individually. This conclusion is supported by a recent study showing that the RA domain of RIAM is unstable without the PH domain (Takala and Ylänne, 2012). These observations force a reinterpretation of results in published studies using the RA or PH domains expressed alone (Ménasché et al., 2007) and suggested that we could not readily express the RA and PH domains separately to parse their individual contributions to membrane binding. To circumvent this problem, we expressed tandem RIAM RA-PH domains in which combinations of the binding motifs could be rendered nonfunctional by point mutations. These experiments revealed important characteristics of the two membrane association domains. First, whereas the tandem RA domains separated by a flexible linker could not anchor GFP at the PM, the tandem PH domains could. This suggests that the added affinity and avidity of dual PH domains is sufficient for binding to endogenous levels of $PI(4,5)P_2$, whereas even tandem RA domains fall below the affinity threshold for membranes that display activated Rap1. Besides simple differences in affinity, the abundance and mobility of GTP-bound Rap1 and $PI(4,5)P_2$ in the plane of the membrane are likely to be markedly different, which may contribute to the different relative contributions of the two binding domains.

Second, and more important, experiments with duplicate RA-PH domains demonstrated that the RIAM RA-PH integrated structural unit is more efficient at colocalizing with activated Rap1 than are separated RA and PH domains. Having dual membrane targeting motifs constitutes a proximity detector that affords a higher level of regulation than can be achieved with a single binding motif (Lemmon, 2008). It seems plausible that the evolutionary advantage of the structurally integrated RA-PH domains is that the interaction of the PH domain with membrane enriched in $PI(4,5,)P_2$ spatially positions the RA domain for facile interaction with PM-tethered Rap1. In a beads-on-a-string model, with the PH domain bound to the PM, the independent RA domain would adopt multiple positions and orientations, some of which would not be compatible with Rap1 binding.

Our data clearly show that the isolated RA-PH domain of RIAM translocates to the lymphocyte PM much more efficiently than does full-length RIAM. This suggests that the RA-PH domains are inhibited in full-length RIAM. Using truncation mutants, we mapped the autoinhibitory region to the first 57 residues that precede the two N-terminal coiled-coil regions. Because coiled-coil regions are often involved in intra- and intermolecular protein–protein interactions (Mason and Arndt, 2004), which can be used for autoinhibition of functional domains (Rosenberg et al., 2005), it is plausible that hetero- or homo-multimerization of RIAM is responsible for obscuring the RA-PH membrane-binding module. If this is the case, then some aspect of inside-out signaling to LFA-1 in lymphocytes must disinhibit the RIAM RA-PH domains. Because talin binds to the RIAM N terminus, it is tempting to speculate that talin binding to RIAM might accomplish this conformational change (Fig. 8). Because talin is also autoinhibited (Goksoy et al., 2008), it is possible that RIAM and talin work reciprocally to disinhibit each other. Because RIAM binds to both the inner leaflet of the PM and to the β chain of LFA-1 (Kliche et al., 2012), our model links LFA-1 to talin through membrane-associated RIAM, which would constitute a secondary association in addition to direct binding of talin to the β chain of the integrin (Tadokoro et al., 2003). However, this model still leaves open the question of what aspect of signaling enables talin binding to RIAM.

The immune system can be likened to a double-edged sword. On the one hand, vertebrates cannot survive without it in a world swarming with microbes. On the other hand, it possesses the power to destroy normal tissues. That is, there is a fine balance between host defense and autoimmunity. Lymphocyte adhesion to endothelium and APCs is absolutely required for adaptive immunity and therefore must be tightly controlled. This may explain why RIAM, a molecule which regulates lymphocyte adhesion, is controlled by dual membrane targeting domains that constitute an AND gate rather than a single determinant that would represent a simple switch.

Materials and methods

Cell culture, transfection, and stimulation

Jurkat T cells were obtained from American Type Culture Collection. Cells were maintained in 5% CO_2 at 37°C in RPMI 1640 media supplemented with 10% FBS. Transfection of Jurkats was performed with Lipofectamine 2000 (Invitrogen) according to the manufacturer's instructions, and cells were imaged 24 h later. COS-1 cells (American Type Culture Collection) were maintained in 5% CO_2 at 37°C in DME media supplemented with 10% FBS, 50 U/ml penicillin G, and 50 µg/ml streptomycin. Transfection of COS-1 cells was performed with SuperFect (QIAGEN) according to the manufacturer's instructions. 18 h later, cells were either harvested for lysis or imaged live. Jurkat T cells were stimulated with mouse anti–human CD3 antibody (R&D Systems) at 100 ng/ml. COS-1 cells were stimulated with EGF (Sigma-Aldrich) at 50 ng/ml. Heterodimerization of FKBP12 and FRB constructs was induced by the addition of 500 nM Rapamycin (Sigma-Aldrich). Stimulation of the AT1a receptor was accomplished by the addition of 1 µM angiotensin II (Sigma-Aldrich).

Stimulation, antibodies, and Western blotting

Jurkat T cells were serum starved for 4 h, treated with Wortmannin (Sigma-Aldrich) or vehicle control for 30 min where indicated, and stimulated for 5 min with anti–human CD3 antibody. Cells were directly lysed in 2× Laemmli sample buffer or subjected to subcellular fractionation (see next section). Samples were subjected to SDS-PAGE followed by immunoblotting on nitrocellulose. Antibodies were diluted with and blots were washed with PBST (PBS + 0.1% Tween 20). Analysis for RIAM and RhoGDI were performed with antibodies (1:1,000, Abcam; or 1:1,000, Santa Cruz Biotechnology, Inc., respectively). Phospho-AKT (Ser 473) was monitored by immunoblot using a phosphospecific antibody (Cell Signaling Technology) at a dilution of 1:1,000. Total Erk2 (Santa Cruz Biotechnology, Inc.) was used as a loading control (1:2,000). Anti-GFP (Roche) was used (1:1,000) for immunoblotting of GST pulldowns. Membranes were blocked with blocking buffer (LI-COR Biosciences) and blotted with the indicated antibodies. Blots were developed by incubating with either IRDye 800CW conjugated goat anti–mouse or IRDye 680LT conjugated goat anti–rabbit secondary antibodies (LI-COR) used at (1:20,000). Blots were visualized with an Odyssey Infrared Imaging System (LI-COR Biosciences).

Cell fractionation

Jurkat T cells were resuspended in relaxation buffer (10 mM Pipes, pH 7.3, 100 mM KCl, 3 mM NaCl, 3.5 mM $MgCl_2$, and protease inhibitors) at a concentration of 10^8 cells/ml and subjected to nitrogen cavitation as we

have previously described (Mor et al., 2009). In brief, the cell suspension was equilibrated with N_2 at 350 psi for 20 min at 4°C in a nitrogen bomb (Parr Instrument Company). Dropwise release from the bomb resulted in disruption of the cells by cavitation. The cavitate was collected into a tube containing EDTA to a final concentration of 1 mM and centrifuged at 500 *g* for 10 min to remove unbroken cells and nuclei. Postnuclear supernatants were separated into membrane and cytosolic fractions by centrifugation at 175,000 *g* for 45 min at 4°C. Equal cells equivalents of each fraction were analyzed by SDS-PAGE and immunoblot.

Microscopy

Live cells were plated in 35-mm dishes containing a no. 0 glass coverslip over a 15-mm cutout (MatTek Corporation). COS-1 cells were plated and subsequently transfected in MatTek dishes. Jurkat T cells were transfected in suspension and plated on poly-lysine–coated MatTek dishes before imaging. COS-1 cells and Jurkat T cells were imaged in DME media and RPMI 1640 media, respectively. Cells were imaged at 37°C with an inverted laser-scanning confocal microscope (510 Meta; Carl Zeiss) equipped with a Plan-Apochromat 63×/1.40 oil DIC objective. Images were acquired with Zen 2008 software (Carl Zeiss) and were processed with Photoshop CS4 (Adobe).

Cell adhesion assay

10^6 Jurkat cells were resuspended in 0.4 ml RPMI-1640 medium supplemented with 10% FCS (RPMI-10) and transfected with 50 µg of plasmid DNA encoding various RIAM constructs using an electroporator (Bio-Rad Laboratories) with a 4-mm cuvette and exponential decay pulse set at 250 V, 975 µF, 400 Ohms. The cells were then allowed to recover for 48 h. 96-well flat-bottom MaxiSorp plates (Thermo Fisher Scientific) were coated overnight at 4°C with 10 µg/ml goat anti–human IgG (Jackson ImmunoResearch Laboratories), followed by coating with 1 µg/ml human recombinant ICAM-1/Fc chimera (R&D Systems) or 2% BSA (Sigma-Aldrich) for 1 h at 37°C. Jurkat cells were harvested 48 h after transfection and resuspended as 0.2×10^6/ml in warm PBS and labeled with 1 µM BCECF (Molecular Probes) for 30 min at 37°C, washed in PBS, and resuspended in prewarmed RPMI-10. Cells where then stimulated with either 5 µg/ml anti-CD3 mAbs (Fitzgerald Industries) or with 100 ng/ml PMA for 30 min at 37°C, and then cells were plated in triplicates (100,000 cells/well) and incubated for 1 h at 37°C. Total fluorescence input (Ex494/Em517nm) was determined using a plate reader (SpectraMax M5; Molecular Devices). Unbound cells were removed by washing the plate with warm 0.2% BSA in PBS. Adherence was calculated as emission of bound cells divided by emission of total cells seeded per well.

GST pulldowns

Full-length Rap1b or H-Ras was cloned into pGEX-2T. The resulting plasmids were used to transform BL21 DE3 *E. coli*. Cultures were grown at room temperature and allowed to reach an OD600 of 0.6 before being induced with 1 mM isopropyl-thiogalactopyranoside (IPTG) overnight. Cultures were harvested by centrifugation at 6,000 *g* for 15 min. The cell pellet was resuspended in bacterial lysis buffer (0.5% Triton X-100, 50 mM Tris-Cl, pH 8.0, and 50 mM EDTA) to which a fresh 5 mM DTT and complete protease inhibitor cocktail (Roche) was added. Cells were lysed by the addition of 25 mg lysozyme and allowed to incubate on ice for 20 min. Cells were further disrupted by sonication. The lysed cells were then centrifuged at 20,000 *g* for 30 min. The supernatant was collected and incubated with glutathione-conjugated agarose beads for 60 min at 4°C with gentle agitation. Beads were washed 3× with bacterial wash buffer (0.5% Triton X-100, 20 mM Tris-Cl, pH 8.0, and 500 mM NaCl), and then once with PBS and stored in PBS with protease inhibitor. SDS-PAGE and Coomassie staining were used to determine yield and purity. Nucleotide loading was accomplished by incubating 100 µl GST-Rap1 or GST-H-Ras beads in PBS supplemented with 25 mM EDTA and 0.5 mM GTPγS or GDPβS (Sigma-Aldrich) and allowing it to incubate at room temperature for 15 min. 10 µl of 1 M $MgCl_2$ was added to the reaction and incubated at room temperature for an additional 10 min. COS-1 cells were transfected with the indicated GFP-RIAM construct with Superfect. Cells were lysed 18 h later by the addition of lysis buffer (1% Triton X-100, 20 mM Tris-HCl, pH 7.5, 150 mM NaCl, and 10 mM $MgCl_2$) supplemented with protease inhibitor cocktail. Cleared lysates were divided and incubated with nucleotide-loaded GST-Rap1 or GST-H-Ras for 40 min at 4°C with gentle agitation. Beads were centrifuged at 600 *g* for 2 min and washed 2× with lysis buffer. Samples were then boiled in 2× Laemmli sample buffer and subjected to SDS-PAGE followed by immunoblot analysis with anti-GFP antibodies.

Plasmids

The production of pEGFP-RalGDS-RBD was previously described and consists of the RBD domain of human RalGDS (aa 787–884) cloned into frame after GFP (Bivona et al., 2004). H-Ras12V was subcloned inframe into the BamHI site of pcGN to produce pcGN-H-Ras12V. Rap1 and Rap1V12 were subcloned inframe into pmCherry-C1 (Takara Bio Inc.). cDNA for mouse RIAM (obtained from G. Koretzky, University of Pennsylvania, Philadelphia, PA) was used as a PCR template to produce full-length RIAM and truncations of RIAM that were then cloned into either pEGFP-C1 or pEGFP-N1 vectors (Takara Bio Inc.). Point mutations were made with the QuikChange XL Site-Directed mutagenesis kit (Agilent Technologies). Tandem RA-PH constructs were constructed by sequential cloning of RA-PH into pEGFP-C1. First, an RA-PH construct was cloned into the MCS with EcoR1 and Apa1. A second RA-PH construct was then cloned in with Apa1 and BamH1. A 5-aa linker encoded by the Apa1 site separates the RA-PH constructs. RFP-FKBP12-5-Ptase, RFP-FKBP12, PM-FRB-CFP, and Rat AT1a (gifts of T. Balla, National Institute of Child Health & Human Development, Bethesda, MD) and were previously described (Varnai et al., 2006). RFP-FKBP12 consists of RFP fused to human FKBP12. RFP-FKBP12-5-Ptase consists of RFP fused to human FKBP12 followed by 5-phosphatase domain (aa 214–644) of human type IV 5-phosphatase. PM-FRB-CFP consists of the N-terminal localization sequence of GAP43 (aa 1–20) fused to the FRB domain of mTOR1 (aa 2019–2114) which is also fused to CFP. Rat AT1a was expressed from pcDNA6 myc/his with a C-terminal myc/his tag. PH-PLCδ-GFP (gift of S. Grinstein, Hospital for Sick Children, Toronto, Ontario, Canada) consists of the PH domain from human phospholipase C delta 1 (aa 1–170) fused to GFP. FLAG-Rap1GAP (gift from L. Quilliam, Indiana University School of Medicine, Indianapolis, IN) consists of human Rap1GAP fused to an N-terminal FLAG sequence. All plasmids were verified with bidirectional sequencing.

Protein expression and purification

We generated a 6xHis-tagged RIAM construct by subcloning cDNA encoding residues 149–437 (RA and PH domains) of mouse RIAM into a modified expression vector pET28a (Novagen). We verified the construct by DNA sequencing. We transformed this construct into *E. coli* strain Rosetta2(DE3) (Novagen), and we grew cultures in Luria broth media at 37°C and induced with 0.4 mM (IPTG) at 20°C. We harvested the cells and resuspended them in lysis buffer (20 mM Tris, pH 8.0, and 500 mM NaCl), lysed them by homogenizer, and clarified by centrifugation. We isolated the 6xHis-tagged protein by Ni^{2+}-affinity chromatography, cleaved with TEV protease to remove the tag, and further purified the protein by ion-exchange chromatography (Source S; GE Healthcare). The purified protein included RIAM residues 149–437 and three heterologous residues (GHM) on the N terminus remaining from the TEV protease cleavage site.

X-ray crystallography

We concentrated RIAM RA-PH to 10 mg ml^{-1} and grew crystals at 17°C in hanging drops containing equal volumes of protein solution and reservoir buffer (12% wt/vol PEG3350, 100 mM LiAc). Crystals of RIAM RA-PH belong to space group $P2_1$. There are two RIAM RA-PH molecules in the asymmetric unit (solvent content, 47.4%). We equilibrated crystals in a stabilizing solution containing reservoir buffer plus 20% (vol/vol) ethylene glycol. We collected data from one crystal on beam line X4A at the National Synchrotron Light Source, Brookhaven National Laboratory. We processed diffraction data using HKL2000 (Otwinowski and Minor, 1997) and determined the RIAM RA-PH structure by molecular replacement using the Grb10 RA-PH structure (Depetris et al., 2009; PDB accession no. 3HK0) as the search model. We performed model building with Coot (Emsley and Cowtan, 2004) and refined the structure (at 2.35 Å) using REFMAC (Murshudov et al., 1997). The final atomic model contains residues 178–437, excluding 279–292 (chain A), and residues 179–278, excluding 279–292 (chain B).

Phosphoinositide binding measurements

We mixed purified RIAM RA-PH at concentrations ranging from 0.8 µM to 50 µM, or buffer only, with 12.5 nM (final) BODIPY TMR-labeled phosphoinositides (Echelon) in a buffer containing 20 mM HEPES, pH 7.5, 150 mM NaCl, and 0.05% (vol/vol) Tween-20. After 5 min of incubation, we added 20 µl of the reaction mix to individual wells of a 384-well assay plate (Corning) and then measured fluorescence polarization at room temperature using a plate reader (Infinite F500; TECAN). We used a 535/25 nm filter as an excitation filter, and a pair of 590/20 nm filters as emission polarization filters. We subtracted the buffer-only data from the protein data and performed curve fitting to a single-site (saturating) binding model using SigmaPlot (Systat Software).

Accession Nos.

Atomic coordinates and structure factors for RIAM RA-PH have been deposited in the Protein Data Bank under the accession number 3TCA.

This work was supported by National Institutes of Health Grants CA116034 and GM055279 (to M.R. Philips), DK052916 (to S.R. Hubbard) and AI043552 (to V.A. Boussiotis).

Submitted: 30 January 2012
Accepted: 13 September 2012

References

Bivona, T.G., H.H. Wiener, I.M. Ahearn, J. Silletti, V.K. Chiu, and M.R. Philips. 2004. Rap1 up-regulation and activation on plasma membrane regulates T cell adhesion. *J. Cell Biol.* 164:461–470. http://dx.doi.org/10.1083/jcb.200311093

Bondeva, T., A. Balla, P. Várnai, and T. Balla. 2002. Structural determinants of Ras-Raf interaction analyzed in live cells. *Mol. Biol. Cell*. 13:2323–2333. http://dx.doi.org/10.1091/mbc.E02-01-0019

Calderwood, D.A., R. Zent, R. Grant, D.J. Rees, R.O. Hynes, and M.H. Ginsberg. 1999. The Talin head domain binds to integrin beta subunit cytoplasmic tails and regulates integrin activation. *J. Biol. Chem.* 274:28071–28074. http://dx.doi.org/10.1074/jbc.274.40.28071

Ceccarelli, D.F., I.M. Blasutig, M. Goudreault, Z. Li, J. Ruston, T. Pawson, and F. Sicheri. 2007. Non-canonical interaction of phosphoinositides with pleckstrin homology domains of Tiam1 and ArhGAP9. *J. Biol. Chem.* 282:13864–13874. http://dx.doi.org/10.1074/jbc.M700505200

Chiu, V.K., T. Bivona, A. Hach, J.B. Sajous, J. Silletti, H. Wiener, R.L. Johnson II, A.D. Cox, and M.R. Philips. 2002. Ras signalling on the endoplasmic reticulum and the Golgi. *Nat. Cell Biol.* 4:343–350.

Choy, E., V.K. Chiu, J. Silletti, M. Feoktistov, T. Morimoto, D. Michaelson, I.E. Ivanov, and M.R. Philips. 1999. Endomembrane trafficking of ras: the CAAX motif targets proteins to the ER and Golgi. *Cell*. 98:69–80. http://dx.doi.org/10.1016/S0092-8674(00)80607-8

Depetris, R.S., J. Wu, and S.R. Hubbard. 2009. Structural and functional studies of the Ras-associating and pleckstrin-homology domains of Grb10 and Grb14. *Nat. Struct. Mol. Biol.* 16:833–839. http://dx.doi.org/10.1038/nsmb.1642

Duchniewicz, M., T. Zemojtel, M. Kolanczyk, S. Grossmann, J.S. Scheele, and F.J. Zwartkruis. 2006. Rap1A-deficient T and B cells show impaired integrin-mediated cell adhesion. *Mol. Cell. Biol.* 26:643–653. http://dx.doi.org/10.1128/MCB.26.2.643-653.2006

Dustin, M.L., T.G. Bivona, and M.R. Philips. 2004. Membranes as messengers in T cell adhesion signaling. *Nat. Immunol.* 5:363–372. http://dx.doi.org/10.1038/ni1057

Ebisuno, Y., K. Katagiri, T. Katakai, Y. Ueda, T. Nemoto, H. Inada, J. Nabekura, T. Okada, R. Kannagi, T. Tanaka, et al. 2010. Rap1 controls lymphocyte adhesion cascade and interstitial migration within lymph nodes in RAPL-dependent and -independent manners. *Blood*. 115:804–814. http://dx.doi.org/10.1182/blood-2009-03-211979

Emerson, S.D., V.S. Madison, R.E. Palermo, D.S. Waugh, J.E. Scheffler, K.L. Tsao, S.E. Kiefer, S.P. Liu, and D.C. Fry. 1995. Solution structure of the Ras-binding domain of c-Raf-1 and identification of its Ras interaction surface. *Biochemistry*. 34:6911–6918. http://dx.doi.org/10.1021/bi00021a001

Emsley, P., and K. Cowtan. 2004. Coot: model-building tools for molecular graphics. *Acta Crystallogr. D Biol. Crystallogr.* 60:2126–2132. http://dx.doi.org/10.1107/S0907444904019158

Goksoy, E., Y.Q. Ma, X. Wang, X. Kong, D. Perera, E.F. Plow, and J. Qin. 2008. Structural basis for the autoinhibition of talin in regulating integrin activation. *Mol. Cell*. 31:124–133. http://dx.doi.org/10.1016/j.molcel.2008.06.011

Gureasko, J., W.J. Galush, S. Boykevisch, H. Sondermann, D. Bar-Sagi, J.T. Groves, and J. Kuriyan. 2008. Membrane-dependent signal integration by the Ras activator Son of sevenless. *Nat. Struct. Mol. Biol.* 15:452–461. http://dx.doi.org/10.1038/nsmb.1418

Holt, L.J., and R.J. Daly. 2005. Adapter protein connections: the MRL and Grb7 protein families. *Growth Factors*. 23:193–201. http://dx.doi.org/10.1080/08977190500196267

Huang, L., F. Hofer, G.S. Martin, and S.H. Kim. 1998. Structural basis for the interaction of Ras with RalGDS. *Nat. Struct. Biol.* 5:422–426. http://dx.doi.org/10.1038/nsb0698-422

Isakoff, S.J., T. Cardozo, J. Andreev, Z. Li, K.M. Ferguson, R. Abagyan, M.A. Lemmon, A. Aronheim, and E.Y. Skolnik. 1998. Identification and analysis of PH domain-containing targets of phosphatidylinositol 3-kinase using a novel in vivo assay in yeast. *EMBO J.* 17:5374–5387. http://dx.doi.org/10.1093/emboj/17.18.5374

Katagiri, K., A. Maeda, M. Shimonaka, and T. Kinashi. 2003. RAPL, a Rap1-binding molecule that mediates Rap1-induced adhesion through spatial regulation of LFA-1. *Nat. Immunol.* 4:741–748. http://dx.doi.org/10.1038/ni950

Katagiri, K., N. Ohnishi, K. Kabashima, T. Iyoda, N. Takeda, Y. Shinkai, K. Inaba, and T. Kinashi. 2004. Crucial functions of the Rap1 effector molecule RAPL in lymphocyte and dendritic cell trafficking. *Nat. Immunol.* 5:1045–1051. http://dx.doi.org/10.1038/ni1111

Kiel, C., S. Wohlgemuth, F. Rousseau, J. Schymkowitz, J. Ferkinghoff-Borg, F. Wittinghofer, and L. Serrano. 2005. Recognizing and defining true Ras binding domains II: in silico prediction based on homology modelling and energy calculations. *J. Mol. Biol.* 348:759–775. http://dx.doi.org/10.1016/j.jmb.2005.02.046

Kim, M., C.V. Carman, and T.A. Springer. 2003. Bidirectional transmembrane signaling by cytoplasmic domain separation in integrins. *Science*. 301:1720–1725. http://dx.doi.org/10.1126/science.1084174

Kliche, S., T. Worbs, X. Wang, J. Degen, I. Patzak, B. Meineke, M. Togni, M. Moser, A. Reinhold, F. Kiefer, et al. 2012. CCR7-mediated LFA-1 functions in T cells are regulated by 2 independent ADAP/SKAP55 modules. *Blood*. 119:777–785. http://dx.doi.org/10.1182/blood-2011-06-362269

Lafuente, E.M., A.A. van Puijenbroek, M. Krause, C.V. Carman, G.J. Freeman, A. Berezovskaya, E. Constantine, T.A. Springer, F.B. Gertler, and V.A. Boussiotis. 2004. RIAM, an Ena/VASP and Profilin ligand, interacts with Rap1-GTP and mediates Rap1-induced adhesion. *Dev. Cell*. 7:585–595. http://dx.doi.org/10.1016/j.devcel.2004.07.021

Lee, H.S., C.J. Lim, W. Puzon-McLaughlin, S.J. Shattil, and M.H. Ginsberg. 2009. RIAM activates integrins by linking talin to ras GTPase membrane-targeting sequences. *J. Biol. Chem.* 284:5119–5127. http://dx.doi.org/10.1074/jbc.M807117200

Lemmon, M.A. 2008. Membrane recognition by phospholipid-binding domains. *Nat. Rev. Mol. Cell Biol.* 9:99–111. http://dx.doi.org/10.1038/nrm2328

Mason, J.M., and K.M. Arndt. 2004. Coiled coil domains: stability, specificity, and biological implications. *ChemBioChem*. 5:170–176. http://dx.doi.org/10.1002/cbic.200300781

Ménasché, G., S. Kliche, E.J. Chen, T.E. Stradal, B. Schraven, and G. Koretzky. 2007. RIAM links the ADAP/SKAP-55 signaling module to Rap1, facilitating T-cell-receptor-mediated integrin activation. *Mol. Cell. Biol.* 27:4070–4081. http://dx.doi.org/10.1128/MCB.02011-06

Mor, A., M.L. Dustin, and M.R. Philips. 2007. Small GTPases and LFA-1 reciprocally modulate adhesion and signaling. *Immunol. Rev.* 218:114–125. http://dx.doi.org/10.1111/j.1600-065X.2007.00538.x

Mor, A., J.P. Wynne, I.M. Ahearn, M.L. Dustin, G. Du, and M.R. Philips. 2009. Phospholipase D1 regulates lymphocyte adhesion via upregulation of Rap1 at the plasma membrane. *Mol. Cell. Biol.* 29:3297–3306. http://dx.doi.org/10.1128/MCB.00366-09

Murshudov, G.N., A.A. Vagin, and E.J. Dodson. 1997. Refinement of macromolecular structures by the maximum-likelihood method. *Acta Crystallogr. D Biol. Crystallogr.* 53:240–255. http://dx.doi.org/10.1107/S0907444996012255

Nassar, N., G. Horn, C. Herrmann, A. Scherer, F. McCormick, and A. Wittinghofer. 1995. The 2.2 A crystal structure of the Ras-binding domain of the serine/threonine kinase c-Raf1 in complex with Rap1A and a GTP analogue. *Nature*. 375:554–560. http://dx.doi.org/10.1038/375554a0

Nassar, N., G. Horn, C. Herrmann, C. Block, R. Janknecht, and A. Wittinghofer. 1996. Ras/Rap effector specificity determined by charge reversal. *Nat. Struct. Biol.* 3:723–729. http://dx.doi.org/10.1038/nsb0896-723

Otwinowski, Z., and W. Minor. 1997. Processing of x-ray diffraction data collected in oscillation mode. *Methods Enzymol.* 276:307–326. http://dx.doi.org/10.1016/S0076-6879(97)76066-X

Reedquist, K.A., E. Ross, E.A. Koop, R.M. Wolthuis, F.J. Zwartkruis, Y. van Kooyk, M. Salmon, C.D. Buckley, and J.L. Bos. 2000. The small GTPase, Rap1, mediates CD31-induced integrin adhesion. *J. Cell Biol.* 148:1151–1158. http://dx.doi.org/10.1083/jcb.148.6.1151

Rosenberg, O.S., S. Deindl, R.J. Sung, A.C. Nairn, and J. Kuriyan. 2005. Structure of the autoinhibited kinase domain of CaMKII and SAXS analysis of the holoenzyme. *Cell*. 123:849–860. http://dx.doi.org/10.1016/j.cell.2005.10.029

Schürpf, T., and T.A. Springer. 2011. Regulation of integrin affinity on cell surfaces. *EMBO J.* 30:4712–4727. http://dx.doi.org/10.1038/emboj.2011.333

Stacey, D.W., L.A. Feig, and J.B. Gibbs. 1991. Dominant inhibitory Ras mutants selectively inhibit the activity of either cellular or oncogenic Ras. *Mol. Cell. Biol.* 11:4053–4064.

Tadokoro, S., S.J. Shattil, K. Eto, V. Tai, R.C. Liddington, J.M. de Pereda, M.H. Ginsberg, and D.A. Calderwood. 2003. Talin binding to integrin beta tails: a final common step in integrin activation. *Science*. 302:103–106. http://dx.doi.org/10.1126/science.1086652

Takala, H., and J. Ylänne. 2012. Binding properties and stability of the Ras-association domain of Rap1-GTP interacting adapter molecule (RIAM). *PLoS ONE*. 7:e31955. http://dx.doi.org/10.1371/journal.pone.0031955

Torii, S., M. Kusakabe, T. Yamamoto, M. Maekawa, and E. Nishida. 2004. Sef is a spatial regulator for Ras/MAP kinase signaling. *Dev. Cell.* 7:33–44. http://dx.doi.org/10.1016/j.devcel.2004.05.019

Várnai, P., and T. Balla. 1998. Visualization of phosphoinositides that bind pleckstrin homology domains: calcium- and agonist-induced dynamic changes and relationship to myo-[3H]inositol-labeled phosphoinositide pools. *J. Cell Biol.* 143:501–510. http://dx.doi.org/10.1083/jcb.143.2.501

Varnai, P., B. Thyagarajan, T. Rohacs, and T. Balla. 2006. Rapidly inducible changes in phosphatidylinositol 4,5-bisphosphate levels influence multiple regulatory functions of the lipid in intact living cells. *J. Cell Biol.* 175:377–382. http://dx.doi.org/10.1083/jcb.200607116

Wohlgemuth, S., C. Kiel, A. Krämer, L. Serrano, F. Wittinghofer, and C. Herrmann. 2005. Recognizing and defining true Ras binding domains I: biochemical analysis. *J. Mol. Biol.* 348:741–758. http://dx.doi.org/10.1016/j.jmb.2005.02.048